

Fully Tunable Fano Resonances in Chiral Electronic Transport

Ai-Ying Ye and Zhao Yang Zeng*

Department of Physics, Jiangxi Normal University, Nanchang 330022, China

Fano resonance is believed to arise when a direct path interferes with a resonant path. We demonstrate that this is not true for chiral electronic transmission without additional direct paths. To address the Fano effect in chiral electronic transport, we suggest an electronic Mach-Zehnder-Fano interferometer (MZFI), which combines a quantum dot with an electronic Mach-Zehnder interferometer. Backscattering is completely suppressed in chiral electronic transport, yielding perfect Fano profiles that can be fully adjusted by an external magnetic flux in the transmission, linear conductance, and differential spectra. Even the current and shot noise for a symmetric interferometer with two arms of the same length exhibit fully controllable resonances and distinct Fano resonance characteristics. Along with the profiles, all of the transport spectra follow the same evolution pattern in a cycle that is resistant to changes in the device's defining parameters.

Introduction.— Fano resonance[1], characterized by asymmetric line profiles, is of fundamental and practical interest. It results from interference between one resonant path and one nonresonant (direct) path. The Fano profile is defined as $(\delta + q)^2/(\delta^2 + 1)$, where δ represents the dimensionless detuning and q is the asymmetry parameter. Fano line profiles have been observed in the characteristic spectra of a number of systems, including photoabsorption in atoms[3], neutrons[4] and electrons[5] scattering, Raman scattering[6], photoabsorption in quantum wells[7], scanning tunneling microscopy[8], and conductance through quantum dots QDs[9].

Resonant tunneling through QD devices has drawn a great deal of attention in the last several decades. Conductance peaks in QDs exhibit the Breit-Wigner form $1/(\delta^2 + 1)$ [10, 11], despite strong electron-electron interaction in QDs. One could expect a Fano-type line shape for conductance or transmission probability if a quantum wire is side-coupled to a localized resonant mode[12–15]. The first surprising discovery of the asymmetric line shape of differential conductance occurred in the study of Kondo resonance for tunneling into a surface magnetic atom [8]. Göres et al.[9] conducted a systematic experimental study on the Fano effect in electronic transport through a QD, an electron droplet generated in a two-dimensional electron gas by electrostatic gating, which permits adjusting of resonant width. However, the transition of the conductance dip into a peak by altering the magnetic field is not well understood, and the origin of the nonresonant route is unclear[9, 16]. This work sparked subsequent investigations on Fano resonances in conductance through an Aharonov-Bohm(AB)ring with a QD embedded in one arm[17, 18] and a quantum wire with a side-coupled QD[19–21] in the Coulomb blockade regime, as well as in the Kondo regime[22–27].

There has been little investigation into Fano resonances in chiral electronic transport thus far. Backscattering is entirely suppressed for chiral electrons. Therefore, it is forbidden to embed a QD in a chiral quantum wire. Transmission probability through a chiral channel with a side-coupled resonant mode is always unity, irrespective of the electron's incident energy, and thus no Fano resonance can be expected, in striking contrast to the nonchiral case where the transmission probability develops a Fano dip at resonance [14, 24, 25, 27] due to resonant reflection. However, if we introduce another chiral mode and allow electrons to tunnel into it, electrons will have two paths to choose from, and interference between these two channels could result in an unexpected Fano effect. To achieve this, we assemble the aforementioned elements into an electronic MZFI, which may be the most straightforward configuration to examine the Fano effect in chiral electron transport. Each electron only travels through the MZFI once, simplifying the theoretical analysis and unraveling the underlying physics more clearly

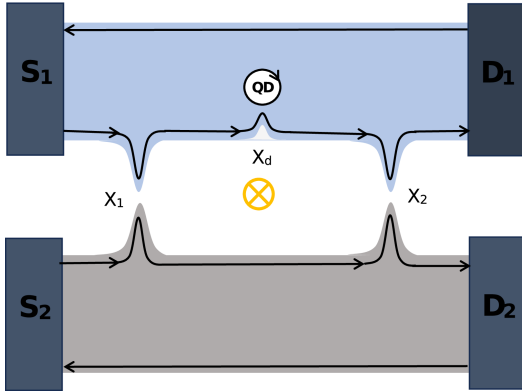


FIG. 1. Schematic illustration of a four-terminal electronic MZFI: Two chiral edge states, represented by arrowhead lines, are formed at the boundaries of two quantum hall fluids of opposite chirality (light blue and light grey regions) at filling factor $\nu = 1$. A QD is etched close to the inner edge of a fluid, enabling electrons to tunnel between the edge and the dot, thus providing the resonant path in the Fano model. QPC1 splits the incoming electron beam from S_1 or S_2 into two portions propagating along the upper and lower arms; QPC2 recombines two portions back together, with resultant outgoing currents collected and measured at D_1 and D_2 . The two arms encircle a magnetic flux Φ and form an AB ring

* zyzeng@hunnu.edu.cn

than any nonchiral interferometer, where electrons traverse forth and back many times before departing.

Model and Formulation.—We consider a four-terminal electronic Mach-Zehnder interferometer (MZI) [28–41] integrated with a QD, schematically shown in Fig. 1, and we call it an electronic MZFI. An electronic MZFI in a quantum Hall liquid at filling factor $\nu = 1$ can be realized through the deposit of elaborately-tailored split metallic gates on the surface of the involved semiconductor heterostructure [28, 31, 37]. Two inner edge states are employed as the chiral modes propagating along the two arms of the interferometer. Ohmic contacts serve as carrier sources (S_1, S_2), each injecting a carrier stream split at x_1 by QPC1 (quantum point contact) to two partial beams. One moves along the upper arm with a nearby QD at x_d , which provides the resonant path in the Fano model, while the other moves down the lower arm. They recombine at x_2 by QPC2 and interfere, resulting in two complementary currents that are collected by another two ohmic contacts functioning as drains (D_1, D_2).

The Hamiltonian model that is being used is $H_\alpha + H_d + H_d + H_{ul} + H_{ud} = \sum_{\alpha=u,l} H_\alpha$. While H_d and H_{ud} explain the localized mode in the QD and coupling between the QD and the upper edge, H_α and H_{ul} reflect the free motion along each edge and interedge electron tunneling. In terms of field operator annihilating an electron at position x on the edge α , $\hat{\psi}_\alpha(x)$, the Hamiltonian of free chiral modes is defined as follows: $H_\alpha = -i\hbar v_F \int dx \hat{\psi}_\alpha^\dagger(x) [\partial_x + ieA_\alpha(x)/\hbar c] \hat{\psi}_\alpha(x)$, where v_F is the Fermi velocity and $A_\alpha(x)$ is the magnetic vector potential experienced by chiral electrons on the edge α at position x . The expression $H_{ul} = \sum_{j=1,2} [t_j \hat{\psi}_u^\dagger(x_j) \hat{\psi}_l(x_j) + t_j^* \hat{\psi}_l^\dagger(x_j) \hat{\psi}_u(x_j)]$, where the tunneling amplitude is $t_j = 2\hbar v_F \gamma_j$. This indicates that electrons can be reflected or transmitted at the positions x_1 and x_2 of the two QPCs. The Hamiltonian $H_d = \epsilon_d \hat{d}^\dagger \hat{d}$ is used to represent the QD. By adjusting the gate bias, one may modify the localized level ϵ_d . The expression $H_{ud} = t_d [\hat{\psi}_u^\dagger(x_d) \hat{d} + \hat{d}^\dagger \hat{\psi}_u(x_d)]$ represents the coupling between the QD and the upper edge. The tunneling amplitude between the upper edge and the QD is expressed as $t_d = \sqrt{2}\hbar v_F \gamma_d / \sqrt{d}$, where d is the characteristic length of the contact. A gauge transformation $\hat{\psi}_\alpha(x) \rightarrow e^{-\frac{ie}{\hbar c} \int_{x_0}^x dx A_\alpha(x)} \hat{\psi}_\alpha(x)$ can be used to extract $A_\alpha(x)$ from the free edge Hamiltonian. The tunneling amplitudes t_j are changed to $t_j e^{\frac{ie}{\hbar c} [\int_{x_0}^{x_j} dx A_u(x) - \int_{x_0}^{x_j} dx A_l(x)]}$ under the gauge transformation.

We calculate the current I_{D_1} flowing into drain 1, using the equation-of-motion method in real space and the Keldysh technique (for details, See the supplementary material [42]), and find

$$I_{D_1} = I_{D_1}^0 + \frac{e}{h} \int_{-\infty}^{+\infty} d\epsilon [f_{S_2}(\epsilon) - f_{S_1}(\epsilon)] \mathcal{T}_{D_1 S_2}(\epsilon), \quad (1)$$

where

$$I_{D_1}^0 = \frac{e}{h} \int_{-\infty}^{+\infty} d\epsilon [f_{D_1}(\epsilon) - f_{S_1}(\epsilon)] \quad (2)$$

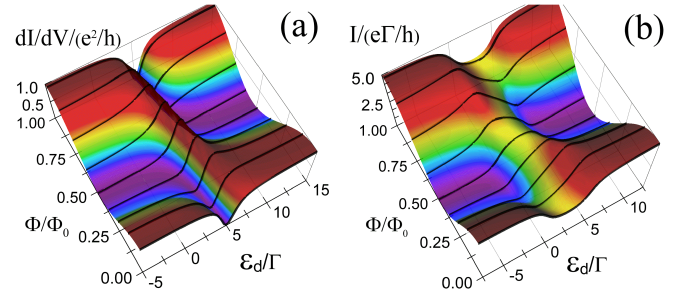


FIG. 2. Differential conductance dI/dV in units of e^2/h (a, left panel) and current I in units of $e\Gamma/h$ (b, right panel) at zero temperature are plotted as functions of the dot level ϵ_d/Γ with varying magnetic flux Φ/Φ_0 . The parameters are: $T_1 = T_2 = 0.5$, $eV/\Gamma = 5$.

is the direct current from S_1 to D_1 without interedge and edge-dot tunneling, and

$$\mathcal{T}_{D_1 S_2}(\epsilon) = |\sqrt{R_1 T_2} + \sqrt{T_1 R_2} \tau_d(\epsilon) e^{-i\phi}|^2 \quad (3)$$

is the transmission probability from lead S_2 to lead D_1 . Here $T_i = 4\gamma_i^2/(1+\gamma_i^2)^2$ and $R_i = (1-\gamma_i^2)^2/(1+\gamma_i^2)^2$ are the transmission and reflection coefficients of the QPCi, respectively; $\phi = \phi_{AB} + \phi_L$, $\phi_{AB} = 2\pi \frac{\Phi}{\Phi_0}$ is the AB phase with Φ being the magnetic flux enclosed by two arms of the interferometer and $\Phi_0 = hc/e$ the flux quantum, and $\phi_L = \epsilon \Delta L / \hbar v_F$ is the phase shift resulting from the length difference $\Delta L = L_l - L_u$ of the two arms; $\tau_d(\epsilon) = \frac{\epsilon - \epsilon_d - i\Gamma}{\epsilon - \epsilon_d + i\Gamma}$ is the transmission amplitude through the position x_d where the QD is coupled, with $\Gamma = \hbar v_F \gamma_d^2 / d$ the width of the resonant level ϵ_d . It should be noted that, instead of 1, the value of the heaviside function $\theta(x)$ at zero is assumed to be $1/2$, or $\theta(0) = 1/2$. It produces the retarded Green's functions of free edge α $g_{\alpha\alpha}^r(x, x) = 1/(2i\hbar v_F)$, which leads to the above expression for $\tau_d(\epsilon)$ throughout this study. This assumption is supported within the scattering matrix approach [42].

Eq. (1) shows that when both edges are coupled to the same source and drain only direct current persists, suggesting that quantization of the Hall conductance is independent of interedge tunneling and impurity scattering. For this reason, we will concentrate on the case in which $\mu_{S_1} = \mu_{D_1} = 0$, $\mu_{S_2} = \mu_{D_2} = eV$ is achieved by setting the electrochemical potentials of four contacts in this manner. The current originating from S_2 , denoted by $I = I_{D_1} = \frac{e}{h} \int d\epsilon [f(\epsilon - eV) - f(\epsilon)] \mathcal{T}_{D_1 S_2}(\epsilon)$, is the only nonzero current.

Transmission.— By defining a background transmission probability without edge-dot tunneling, $\mathcal{T}_{D_1 S_2}^0(\phi) = |\sqrt{R_1 T_2} + \sqrt{T_1 R_2} e^{-i\phi}|^2$, and $\mathcal{A} = \sqrt{T_1 R_1 T_2 R_2}$, the transmission probability can be expressed in terms of a dimensionless detuning $\delta(\epsilon) = (\epsilon - \epsilon_d)/\Gamma$ as

$$\mathcal{T}_{D_1 S_2}(\epsilon) = \mathcal{T}_{D_1 S_2}^0(\phi) - 4\mathcal{A} \frac{\sin\phi \delta(\epsilon) + \cos\phi}{\delta^2(\epsilon) + 1}. \quad (4)$$

Fano resonance is seen in the profile term of Eq. (4), where the antisymmetric part $\delta(\epsilon)/[\delta^2(\epsilon) + 1]$ is repre-

sented by a peak at $\delta(\epsilon) = 1$ and a dip at $\delta(\epsilon) = -1$, and the symmetric part $1/[\delta^2(\epsilon) + 1]$ is characterized by a peak of width 2 at $\delta(\epsilon) = 0$. Since $\phi = 0$, this transmission probability exhibits a symmetric dip that is specific to Fano resonance and fits neatly into the Fano profile.

$$\mathcal{T}_{D_1 S_2}(\epsilon) = \mathcal{T}_{D_1 S_2}^0(\pi) + \frac{4\mathcal{A}}{1 + q^2(\phi)} \frac{[\delta(\epsilon) + q(\phi)]^2}{\delta^2(\epsilon) + 1}, \quad (5)$$

where the Fano asymmetry parameter is denoted by $q(\phi) = -\tan(\phi/2)$. In the transmission profile, Eq. (5) predicts one minimum at $\delta(\epsilon) = -q(\phi)$ and one maximum at $\delta(\epsilon) = 1/q(\phi)$. If $q = 0$, this reduces to a single symmetric peak; if $q \rightarrow \pm\infty$, it reduces to a single symmetric dip. In terms of the transmission phase $\phi_d(\epsilon) = \arctan[2\delta(\epsilon)/(1 - \delta^2(\epsilon))] - \pi$, the unity modulus of the transmission amplitude $\tau_d(\epsilon)$ admits an exponential expression $\tau_d(\epsilon) = e^{i\phi_d(\epsilon)}$. This leaves us with a well-known expression for the transmission probability $\mathcal{T}_{D_1 S_2} = |\sqrt{R_1 T_2} + \sqrt{T_1 R_2} e^{i[\phi_d(\epsilon) - \phi]}|^2$. Constructive or destructive interference takes place when the phase difference $\phi_d(\epsilon) - \phi$ is 0 or π . The location of the maxima and minima in the transmission spectrum can be found using the inverse trigonometric function relations $2\arctan(x) = \arctan[2x/(1 - x^2)]$, $x^2 < 1$ and $\arctan(x) + \operatorname{arccot}(x) = \pi/2$. These relations are equivalent to the condition of constructive or destructive interference. If we additionally assume a symmetric interferometer, $\Delta L = 0$, the Fano asymmetry parameter $q = -\tan(\phi_{AB}/2)$ becomes just a function of the AB phase. Consequently, it is possible to fully tune Fano resonances in the transmission and linear conductance spectra of the MZFI by simply tuning it to be any real number by altering an external magnetic flux.

Current and conductance— At zero temperature, the current is given by

$$I = \frac{e\Gamma}{h} \left[\mathcal{T}_{D_1 S_2}^0(\phi_{AB}) \frac{eV}{\Gamma} - 4\mathcal{A} \left[\frac{\sin\phi_{AB}}{2} \ln(\delta^2(\epsilon) + 1) + \cos\phi_{AB} \arctan\delta(\epsilon) \right] \Big|_0^{eV} \right], \quad (6)$$

where $f(\epsilon)|_b^a = f(a) - f(b)$, and the differential conductance is calculated as

$$\frac{dI}{dV} = \frac{e^2}{h} \left[\mathcal{T}_{D_1 S_2}^0(\phi_{AB}) - 4\mathcal{A} \frac{\sin\phi_{AB}\delta(eV) + \cos\phi_{AB}}{\delta^2(eV) + 1} \right], \quad (7)$$

which can be also expressed as $\frac{dI}{dV} = \frac{e^2}{h} \mathcal{T}_{D_1 S_2}(eV)$.

Although their profiles appear to be quite different, the differential conductance and current are the same type of oscillatory functions of the AB phase with period 2π as the transmission probability, performing identical profile evolution as the AB phase grows. However, because the

current is the integration of the transmission probability over energy from 0 to eV , we will immediately see that their profiles are closely related. The applied voltage V appears to have an effect on the current distribution. The profile function in Eq. (6) shows two unique behaviors: the arctangent terms act as the symmetric component, resulting in a peak at $\epsilon_d = eV/2$ that broadens with rising eV , and the logarithmic terms behave as the anti-symmetric part, admitting a dip at $\epsilon_d = eV$ and a peak at $\epsilon_d = 0$. Because of the cumulative effect of integration, the present profiles can be seen as enlarged versions of the transmission profiles.

In actual experiments, it is more convenient to modify the resonant level ϵ_d while fixing the voltage V by varying the bias voltage to the plunger gate of the dot. As functions of the dot level ϵ_d and the enclosed magnetic flux Φ/Φ_0 with $eV/\Gamma = 5$, we display the differential conductance in Fig. 2(a) and the current in Fig. 2(b). These may be clearly seen by taking $T_1 = T_2 = 0.5$. The differential conductance and the current, albeit having different profiles, exhibit fully tunable Fano resonances by adjusting the magnetic flux, as predicted. They also show identical profile progression over the increasing magnetic flux. In contrast to the sharp peak-dip pattern in the differential conductance, the accumulation effect causes the peaks and dips in the current spectrum to significantly broaden and appear as arches and valleys, as can be seen in Fig. 2. Observe that for any finite voltage V , the chiral transport is coherent, which is in line with the experimental observation[40] and the theoretical result[33] in the study on decoherence in the electronic MZIs. In our configuration, the QD is an essential component of the coherent transport device as a whole. In contrast to the circumstances [37, 43] where the QD functions as a detecting apparatus, it does not cause any dephasing.

Shot noise.— Due to interference, Fano resonances can be seen in every transmission probability. Fano resonances in the electronic MZFI shot noise are possible. At zero temperature, $\Delta I_{S_1} = \Delta I_{S_2} = 0$, there is no noise in the incident stream according to the coherent scattering theory[45, 46]. The currents flowing into the drain contacts, I_{D_1} and I_{D_2} , are the only ones that fluctuate. Because of current conservation, $\Delta I_{D_1} + \Delta I_{D_2} = 0$ in particular. The transmissions probabilities from S_j to D_i are associated with the scattering matrix elements of the system by $\mathcal{T}_{D_i S_j} = |s_{D_i S_j}|^2$. Flux conservation yields $\sum_{i=1,2} \mathcal{T}_{D_i S_j} = 1$. According to [42], the shot noise power tensor's nonzero components are $S = S_{D_1 D_1} = S_{D_2 D_2} = -S_{D_1 D_2} = -S_{D_2 D_1}$ and are provided by

$$S = \frac{e^2}{\pi h} \int_0^{eV} d\epsilon \mathcal{T}_{D_1 S_2}(\epsilon) \mathcal{T}_{D_2 S_2}(\epsilon), \quad (8)$$

which gives differential shot noise

$$\frac{dS}{dV} = \frac{2e^3}{h} \left[\mathcal{T}_{D_1S_2}^0(\phi_{AB})\mathcal{T}_{D_2S_2}^0(\phi_{AB}) + 8\mathcal{A}^2 [\cos(2\phi_{AB}) \frac{2\delta^2(eV)}{[\delta^2(eV) + 1]^2} + \sin(2\phi_{AB}) \frac{\delta(eV)[\delta^2(eV) - 1]}{[\delta^2(eV) + 1]^2}] \right], \quad (9)$$

and shot noise

$$S = \frac{e^2\Gamma}{h} \left[\mathcal{T}_{D_1S_2}^0(\phi_{AB})\mathcal{T}_{D_2S_2}^0(\phi_{AB}) \frac{eV}{\Gamma} + 8\mathcal{A}^2 [\cos(2\phi_{AB})P_S(\epsilon_d, eV) + \sin(2\phi_{AB})P_A(\epsilon_d, eV)] \right], \quad (10)$$

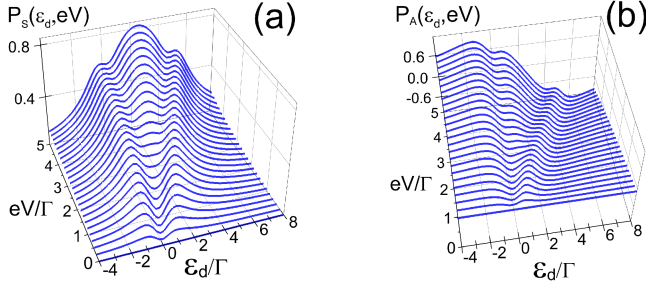


FIG. 3. Evolution of symmetric $P_S(\epsilon, eV)$ (a, left panel) and antisymmetric $P_A(\epsilon, eV)$ (b, right panel) parts of the profile function in shot noise as the voltage eV increases from 0 to 5Γ .

where $\mathcal{T}_{D_2S_2}^0$ is defined similar to $\mathcal{T}_{D_1S_2}^0$, $P_S(\epsilon_d, eV) = [\arctan\delta(\epsilon) - \delta(\epsilon)/[\delta^2(\epsilon) + 1]]|_0^{eV}$ and $P_A(\epsilon_d, eV) = [1/[\delta^2(\epsilon) + 1] + \ln[\delta^2(\epsilon) + 1]/2]|_0^{eV}$ are the symmetric and antisymmetric parts of the profile function of the shot noise. As functions of AB phase, the differential shot noise and shot noise execute the identical oscillation with halved period π . The ratio of the shot noise to the Poisson noise, $F = S/S_P = S/2eI$, is known as the Fano factor. An equivalent definition of a differential Fano factor is $F_d = (dS/dV)/2e(dI/dV)$. If the QD is taken out of the device, these two factors coincide and reduce to $F^0 = F_d^0 = \mathcal{T}_{D_2S_2}^0 = |\sqrt{R_1R_2} - \sqrt{T_1T_2}e^{-i\phi_{AB}}|^2$, which is always no greater than 1 and exhibit AB oscillations. Once the QD is involved, the Fano factor F evolves in a complicated way, while the differential Fano factor F_d remains rather simple and acquires the form of the transmission $\mathcal{T}_{D_2S_2}(eV)$, thus showing perfect Fano resonances.

The product of the two transmission probabilities, $\mathcal{T}_{D_1S_2}(eV)$ and $\mathcal{T}_{D_2S_2}(eV)$, determines the differential shot noise. It takes maximum values when one of the transmission probabilities is halfway between its maximum and minimum, and minimum values when either of the two coefficients is either maximal or minimal. As a result, the differential shot noise spectrum now shows dips where the differential conductance spectrum showed peaks or dips. The locations in the differential conductance spectra that correspond to a point halfway between the ridge and the valley should show peaks of differential shot noise. Verification of this intuitive picture can be done by looking at the differential shot noise pro-

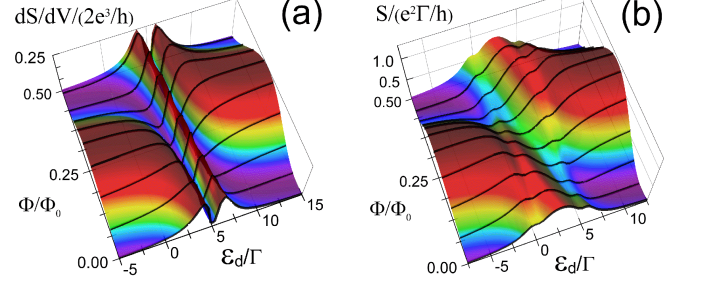


FIG. 4. Differential shot noise dS/dV in units of $2e^3/h$ (a, left panel) and shot noise S in units of $e^2\Gamma/h$ (b, right panel) are plotted as functions of the dot level ϵ_d/Γ with varying magnetic flux Φ/Φ_0 . The parameters are the same as in Fig. 2

file function in Eq. (9), which is reminiscent of the line shapes of complex susceptibility of three-level atomic systems in electromagnetically induced transparency (EIT) phenomenon[44]. EIT, or absorption cancellation, is caused by destructive interference between the two coherent routes for absorption and is comparable to Fano antiresonance. The antisymmetric part of the profile in the sine term admits, on the right side of the $\delta(eV)$ -axis, a sharp dip of depth 0.25 at $\delta(eV) = \sqrt{2} - 1$ and a broad peak of height 0.25 at $\delta(eV) = 1 + \sqrt{2}$. The symmetric part of the profile in the cosine term is peaked symmetrically at $\delta(eV) = \pm 1$ and drops to zero at the midpoint $\delta(eV) = 0$. Depending on ϕ_{AB} , either of these two terms dominates, or both cooperate, resulting in symmetric double-peak or double-dip profiles, or asymmetric profiles with a deformed double-peak or double-dip structure in the differential shot noise spectrum. In the case of shot noise, the symmetric component $P_S(\epsilon, eV)$ has a profile of two or three peaks symmetric about the $\epsilon_d = eV/2$, depending on the ratio of eV/Γ . On the other hand, the antisymmetric component $P_A(\epsilon, eV)$ gives us a profile of a sharp peak with a broad dip on the right and a broad peak on the left as long as $eV/\Gamma < 2$. The sharp peak splits and gradually develops into two side shoulders that are located at $\epsilon_d = 0$ and $\epsilon_d = eV$ as eV is increased. Figures 3(a) and 3(b), respectively, clearly show the evolutions of the symmetric and antisymmetric profiles of the shot noise with increasing voltage eV . We stress that, peculiar to Fano resonances, a profile of symmetric double-peak with a dip at the center $\epsilon_d = eV/2$ and a profile of symmetric double-peak or triple-peak should be

detected in differential shot noise and shot noise spectra of a **MZFI**. We provide profile evolutions of the differential shot noise from Eq. (9) in Fig. 4(a) and shot noise from Eq. (10) in Fig. 4(b), where the magnetic flux Φ/Φ_0 varies from 0 to 0.5. Figures 4(a) and 4(b) support our analytical findings in Eqs. (9) and (10). Furthermore, the evolution patterns in differential shot noise and shot noise are identical to those in differential conductance and current throughout one evolution cycle. The profile evolution of all transport spectra of a **MZFI** is dominated by sine and cosine functions; therefore, this result comes as no surprise.

Asymmetric MZFI—Fano resonances in transport spectra for a symmetric **MZFI** with $\Delta L = 0$ have been the subject of our investigation thus far. Another energy scale, $E_A = \hbar v_F/\Delta L$, will be introduced by interferometer arm asymmetry; for instance, $\Delta L = L_l - L_u > 0$. A replacement $\phi_{AB} \rightarrow \phi_{AB} + eV/E_A$ can be used to explain how the asymmetry in interferometer arm lengths affects differential transport spectra, including differential conductance, differential shot noise, and differential Fano factor. We are interested in the case where there is a slight mismatch between the arm lengths where $E_A \gg eV, \epsilon_d, \Gamma$ for the current and shot noise. The presence of the asymmetry effect is indicated by a slight modification of the symmetric (P_S) and antisymmetric (P_A) parts of the profile function, so that, up to first order in $1/E_A$, $P'_S \approx (1 - \frac{\Gamma}{E_A})P_S + \frac{\epsilon_d}{E_A}P_A$, $P'_A \approx (1 - \frac{\Gamma}{E_A})P_A - \frac{\epsilon_d}{E_A}P_S$ for current, and $P'_S \approx (1 - \frac{2\Gamma}{E_A})P_S + \frac{2\epsilon_d}{E_A}P_A - \frac{2\Gamma}{E_A}\arctan\delta(\epsilon)|_0^{eV}$, $P'_A \approx (1 - \frac{2\Gamma}{E_A})P_A - \frac{2\epsilon_d}{E_A}P_S - \frac{\Gamma}{E_A}\ln[\delta^2(\epsilon) + 1]|_0^{eV}$ for shot noise. The integrations in the current and shot noise formulas cannot be further simplified but can be directly computed numerically if the mismatch ΔL is comparable with eV . In this instance, the shot noise and current profiles will be distorted, but the profile evolution will remain intact.

QD in the Coulomb blockade or Kondo regime—When considering the Coulomb interaction U between electrons in the **QD**, one may question if Fano resonances may be seen in transport spectra of a **MZFI**. We think the formalism is applicable to an interacting resonant level that can be described by a single level Anderson model.

$\tau_d(\epsilon) = 1 - 2i\Gamma g_{dd}^r$ [42] represents the transmission amplitude through the point where a noninteracting **QD** is side coupled, where $g_{dd}^r(\epsilon) = [(g_{dd}^{0r}(\epsilon))^{-1} - \Sigma_d(\epsilon)]^{-1} = (\epsilon - \epsilon_d + i\Gamma)^{-1}$ is the full retarded Green's function of the noninteracting dot. $\tau_d(\epsilon) = \frac{\epsilon - \epsilon_d - i\Gamma}{\epsilon - \epsilon_d + i\Gamma}$ and the transmission probability is always unity. This imposes a strict constraint on the formalism with an interacting **QD**. Changing the Green's function of the isolated **QD** is a clumsy but sensible solution. Under the constraint $Im\Sigma_d(\epsilon) = -i\Gamma$, One can select $Re\Sigma_d(\epsilon) = 0$ and $g_{dd}^{0r}(\epsilon) = (1 - n_d)(\epsilon - \epsilon_d + i0^+)^{-1} + n_d(\epsilon - \epsilon_d - U + i0^+)^{-1}$ in the Coulomb blockade regime[47, 48], $g_{dd}^{0r}(\epsilon) = (\epsilon - \epsilon_d + i0^+)^{-1}$ and $\epsilon - \epsilon_d - Re\Sigma_d(\epsilon) = (\epsilon - \alpha)\Gamma/(2k_B T_K)$ in the Kondo regime[8, 49]. In this case, T_K is the Kondo temperature, α is a constant, and n_d is the occupation number of the resonant level ϵ_d . Thus, one may persuade themselves that even in the case when the **QD** is in the equilibrium Kondo regime or the Coulomb blockade regime, completely tunable Fano resonances could be detected.

Concluding remarks—To summarize, our results indicate that fano resonances require an extra direct path to emerge. Motivated by this finding, we suggest an electronic **MZFI**, which is possibly the simplest and cleanest setting to explore the Fano effect in chiral electronic transport. Despite their simplicity, fully tunable Fano resonances can be easily achieved by altering an external magnetic field in almost all transport spectra of this simple arrangement. They are robust with respect to device parameters such as **QPC** transmission and reflection coefficients, edge-**QD** coupling, and interferometer arm lengths. Therefore, parameters to fit Fano profiles of transport spectra are not needed in chiral electronic transport. Future directions would be of great interest in adapting it to a more intricate edge structure (multi-mode or edge modes in fractional quantum hall systems) and studying the Fano effect in transport through an asymmetric **MZFI** during decoherence. More accurate analytical and numerical approaches could be utilized to examine overlapped Fano resonances with a multi-level **QD** and the Fano effect with a strongly correlated **QD**.

-
- [1] U. Fano, *Phys. Rev.* **124**, 1866 (1961).
[2] A. E. Miroshnichenko, S. Flach, and Y. S. Kivshar, *Rev. Mod. Phys.* **82**, 2257 (2010), M. F. Limonov, M. V. Rybin, A. N. Poddubny, and Y. S. Kivshar, *Nature Photonics* **11**, 543 (2017).
[3] H. Beutler, *Z. Phys.* **93**, 177 (1935).
[4] R. K. Adair, C. K. Bockelman, and R. E. Peterson, *Phys. Rev.* **76**, 308 (1949).
[5] J. A. Simpson and U. Fano, *Phys. Rev. Lett.* **11**, 158 (1963).
[6] F. Cerdeira, T. A. Fjeldly, and M. Cardona, *Phys. Rev. B* **8**, 4734 (1973).
[7] J. Feist, F. Capasso, C. Sirtori, K. W. West, and L. N. Pfeiffer, *Nature London* **390**, 589 (1997).
[8] V. Madhavan, W. Chen, T. Jamneala, M. F. Crommie, and N. S. Wingreen, *Science* **280**, 567 (1998).
[9] J. Göres, D. Goldhaber-Gordon, S. Heemeyer, and M. A. Kastner, *Phys. Rev. B* **62**, 2188 (2000).
[10] U. Meirav, M. A. Kastner, and S. J. Wind, *Phys. Rev. Lett.* **65**, 771 (1990).
[11] C. W. J. Beenakker, *Phys. Rev. B* **44**, 1646 (1991).
[12] W. Porod, Z. Shao, and C. S. Lent, *Appl. Phys. Lett.* **61**, 1350 (1992).
[13] E. Tekman and F. Bagwell, *Phys. Rev. B* **48**, 2553 (1993).
[14] Z. Shao, W. Porod, and C. S. Lent, *Phys. Rev. B* **49**, 7453 (1994).

- [15] J. U. Nöckel and A. Douglas Stone, *Phys. Rev. B* **50**, 17415 (1994).
- [16] A. A. Clerk, X. Waintal, and P. W. Brouwer, *Phys. Rev. Lett.* **82**, 4636 (2001).
- [17] K. Kobayashi, H. Aikawa, S. Katsumoto, and Y. Iye, *Phys. Rev. Lett.* **88**, 256801 (2002), *Phys. Rev. B* **68**, 235304 (2003).
- [18] A. Aharony, O. E-Wohlman, T. Otsuka, S. katsumoto, H. Aikawa, and K. Kobayashi, *Phys. Rev. B* **73**, 195329 (2006).
- [19] K. Kobayashi, H. Aikawa, A. Sano, S. Katsumoto, and Y. Iye, *Phys. Rev. B* **70**, 035319 (2004).
- [20] A. C. Johnson, C. M. Marcus, M. P. Hanson, and A. C. Gossard, *Phys. Rev. Lett.* **93**, 106803 (2004).
- [21] A. Fuhrer, P. Brusheim, T. Ihn, M. Sigrist, K. Ensslin, W. Wegscheider, and M. Bichler, *Phys. Rev. B* **73**, 205326 (2006).
- [22] B. R. Bulka and P. Stefański, *Phys. Rev. Lett.* **86**, 5128 (2005).
- [23] H. Hofstetter, J. König, and H. Schoeller, *Phys. Rev. Lett.* **87**, 156803 (2005).
- [24] M. E. Torio, K. Hallberg, A. H. Ceccatto, and C. R. Proetto, *Phys. Rev. B* **65**, 085302 (2002).
- [25] A. A. Aligia and C.R. Proetto, *Phys. Rev. B* **65**, 165305 (2002).
- [26] M. Sato, H. Aikawa, S. Katsumoto, and Y. Iye, *Phys. Rev. Lett.* **95**, 066801 (2005).
- [27] K. Kang, S. Y. Cho, J. J. Kim, and S. C. Shin, *Phys. Rev. B* **63**, 113304 (2007).
- [28] Y. Ji, Y. Chung, D. Sprinzak, M. Heiblum, D. Mahalu, and H. Shtrikman, *Nature*, **422**, 415 (2003).
- [29] V. S.-W. Chung, P. Samuelsson, and M. Büttiker, *Phys. Rev. B* **72**, 125320 (2005).
- [30] L. V. Litvin, H.-P. Tranitz, W. Wegscheider, and C. Strunk, *Phys. Rev. B* **75**, 033315 (2007).
- [31] I. Neder, F. Marquardt, M. Heiblum, D. Mahalu, and V. Umansky, *Nat. Phys.* **3**, 534 (2007).
- [32] P. Roulleau, F. Portier, D. C. Glattli, P. Roche, A. Cavanna, G. Faini, U. Genser, and D. Mailly, *Phys. Rev. B* **76**, 161309 (2007).
- [33] E. Sukhorukov and V. Cheianov, *Phys. Rev. Lett.* **99**, 156801 (2007).
- [34] J. T. Chalker, Y. Gefen, and M. Y. Veilletter, *Phys. Rev. B* **76**, 085320 (2007).
- [35] I. P. Levkivskyi and E. V. Sukhorukov, *Phys. Rev. B* **78**, 045322 (2008).
- [36] E. Bieri, M. Weiss, O. Göktas, M. Hauser, C. Schönenberger, and S. Oberholzer, *Phys. Rev. B* **79**, 245324 (2009).
- [37] E. Weisz, H. K. Choi, M. Heiblum, Y. Gefen, V. Umansky, and D. Mahalu, *Phys. Rev. Lett.* **105**, 056803 (2010).
- [38] I. Neder, M. Heiblum, Y. Levinson, D. Mahalu, and V. Umansky, *Phys. Rev. Lett.* **109**, 250401 (2012).
- [39] H. Le Sueur, C. Altimiras, U. Gennser, A. Cavanna, D. Mailly, and F. Pierre, *Phys. Rev. Lett.* **105**, 056803 (2010).
- [40] S. Tewari, P. Roulleau, C. Grenier, F. Portier, A. Cavanna, U. Gennser, D. Mailly, and P. Roche, *Phys. Rev. B* **93**, 035420 (2016).
- [41] E. G. Idrisov, I. P. Levkivskyi, and E. V. Sukhorukov, *Phys. Rev. Lett.* **121**, 026802 (2018).
- [42] See Supplemental material for technical details on the derivation of various Green's functions, current, scattering matrix and shot noise.
- [43] E. Buks, R. Schuster, M. Heiblum, D. Mahalu, and V. Umansky, *Nature*, **391**, 871 (1998), D. Sprinzak, E. Buks, M. Heiblum and H. Shtrikman, *Phys. Rev. Lett.* **84**, 5820 (2000).
- [44] M. Scully and M. S. Zubairy, *Quantum optics*, Cambridge University Press (1997).
- [45] M. Büttiker, *Phys. Rev. Lett.* **65**, 2901(1990), *Phys. Rev. B* **46**, 12485 (1992).
- [46] Y. M. Blanter and M. Büttiker, *Phys. Rep.* **336**, 1 (2000).
- [47] Y. Meir, N. S. Wingreen, and P. A. Lee, *Phys. Rev. Lett.* **66**, 3048 (1991).
- [48] H. J. W. Haug, and A-P Jauho, *Quantum kinetics in transport and optics of semiconductos*, second edition, Springer (2008).
- [49] A. Houghton, N. Read, H. Won, *Phys. Rev. B* **35**, 5123 (1987).